

BART Streams: Real-time Reconstruction Using a Modular Framework for Pipeline Processing

Philip Schaten^{1,2}, Moritz Blumenthal^{1,3}, Bernhard Rapp¹,
Christina Unterberg-Buchwald^{2,4,5}, and Martin Uecker^{1,2,4,6}

¹Institute of Biomedical Imaging, Graz University of Technology, Graz, Austria

²Institute for Diagnostic and Interventional Radiology, University Medical Center Göttingen, Germany

³Department of Radiology, Boston Children's Hospital, Harvard Medical School, Boston, USA

⁴German Centre for Cardiovascular Research (DZHK), partner site Lower Saxony, Germany

⁵Clinic for Cardiology and Pneumology, University Medical Center Göttingen, Germany

⁶BioTechMed-Graz, Graz, Austria

March 30, 2026

Abstract

Purpose: To create modular solutions for interactive real-time MRI using reconstruction algorithms implemented in BART.

Methods: A new protocol for streaming of multidimensional arrays is presented and integrated into BART. The new functionality is demonstrated using examples for cardiac interactive real-time MRI based on radial FLASH, where iterative reconstruction is combined with advanced features such as dynamic coil compression and gradient-delay correction. We analyze the latency of the reconstruction and measure end-to-end latency of the full imaging process.

Results: Reconstruction pipelines with iterative reconstruction and advanced functionality were built in a modular way using scripting. Latency measurements demonstrate latency sufficient for interactive real-time MRI, on the order of 30 ms for BART processing and network transfer time, or 200 ms for end-to-end latency including acquisition, vendor processing, and display.

Conclusion: With the new streaming capabilities, real-time reconstruction pipelines can be assembled using BART in a flexible way, enabling rapid prototyping of advanced applications such as interactive real-time MRI.

Keywords: MRI, Streaming, Real-Time MRI, Real-Time Reconstruction, Interventional MRI

1 Introduction

“Live streams” from inside the human body were possible for a long time [1] through the combination of real-time MRI acquisition, real-time reconstruction and low-latency visualization. We refer to this as interactive real-time MRI (RT-MRI) [2, 3]. It is an important tool with emerging clinical applications, such as interventional [4–8] or fetal MRI [9]. RT-MRI usually requires high frame rates, e. g. to resolve cardiac motion [10], speech production [11, 12], or joint motion [13]. Thus, RT-MRI often makes use of data undersampling in combination with specific reconstruction methods, for example view-sharing [1], parallel imaging [14], compressed sensing [15, 16], Kalman filtering [17], spatiotemporally constrained reconstruction [18], or other.

In this work, we show examples using the real-time regularized non-linear inversion (RT-NLINV) algorithm [19, 20]. Based on classic regularized non-linear inversion (NLINV) [21], RT-NLINV offers particularly high undersampling factors and is causal, i. e. it does not rely on data acquired after the frame that is currently being reconstructed. Running iterative RT-MRI reconstruction algorithms such as RT-NLINV in real-time typically requires optimized software and hardware acceleration e. g. through the use of Graphical Processing Units (GPU) [22–24], especially when low latency is required. For example, cardiac interventional MRI and MRI-guided radiotherapy might require a latency as low as several 100 ms [7, 25], and speech biofeedback studies were performed with a latency of 100 ms [26].

The BART toolbox for computational MRI [27] is a comprehensive framework which provides a wide range of reconstruction, calibration [28], machine-learning [29, 30], and signal processing tools. Its optimized code and its existing support for GPU computing make it an ideal choice for the development of real-time reconstruction methods. Another core feature of BART is its modular design as a toolbox: Algorithms are made available as individual command line tools, enabling the construction of powerful reconstruction pipeline by combining the different tools in a script. However, high-quality, low latency RT-MRI requires not only optimized reconstruction, but also the ability to stream the data and reconstructed images during the measurement. Each tool in the reconstruction pipeline needs to perform its task as soon as a raw-data frame is available, as opposed to waiting for a complete dataset. Existing software such as the Gadgetron [31], can stream data in ISMRMRD format [32], and BART has been used with Gadgetron in the past [33, 34]. However, up to now, it was not possible to use BART to construct low-latency processing pipelines.

In this work, we integrate new stream processing capabilities into BART. The new functionality facilitates building reconstruction pipelines suitable for RT-MRI with existing BART tools. Importantly, our approach to streaming builds on standard Unix system utilities, which allows us to preserve the full modularity of BART. This is demonstrated using examples for interactive real-time MRI based on radial FLASH, where iterative reconstruction is combined with advanced features such as dynamic coil compression and gradient-delay correction. In particular, we show how the RT-NLINV algorithm implemented in BART can now be used in real-time reconstruction pipelines, and how a

streaming version of geometric coil compression [35] acquires a new use as dynamic coil compression for interactive RT-MRI. Additionally, we analyze the latency of the reconstruction itself and measure the end-to-end latency of the complete imaging process.

2 Methods

We will first give an overview over the architecture of BART, then discuss multi-dimensional arrays, and then explain the new support for looping, and streaming, which is then used for real-time processing.

2.1 BART Structure

BART is a modular reconstruction framework which enables building complex reconstruction algorithms through combination of various individual components. On the lowest level, a numeric library provides generic functions for operations on multidimensional arrays (*md-arrays*). Many of these operations can be accelerated using GPUs, or with the Message Passing Interface (MPI) [36] toolkit, enabling distributed computing on scientific high-performance clusters and multi-GPU usage [37]. The multi-dimensional operations are complemented by an operator library, which provides a simple way of constructing operators, e. g. the forward operator describing an MRI measurement, while automatically providing its adjoint in the case of a linear operator, or the derivative for non-linear operators.

For most use cases it is sufficient to interact with BART using its command line interface, which consists of a set of high-level tools operating on md-arrays. All commands take several individual options and typically input and output file names. A single driver command, `bart`, acts as the unified entry point to BARTs command line interface. It can be called directly from a command line or from scripting languages such as BASH, Python or Matlab. The `bart` call is followed by a set of general options and the name of the tool which should be run. There are basic tools such as `fft` which calculates the Fourier transform of an md-array, as well as many commands for MRI-specific tasks such as whitening (`whiten`), coil compression (`cc`), calibration of sensitivities (`ecalib`, `ncalib`), parallel imaging and compressed sensing (`pics`), model-based reconstruction (`moba`), machine-learning reconstruction (`reconet`, `nlinvnet`), and much more.

The tools act as building blocks and can be combined in a modular way to construct advanced reconstruction pipelines for all kinds of MRI applications. A complete reconstruction implemented with BART thus typically consists of a script that calls various BART commands that operate on md-arrays. For real-time reconstruction, it must be possible to split up, i.e. slice, the multi-dimensional input space and process each subset of the data as it becomes available. In other words, the reconstruction script has to be organized as a pipeline. To support this in BART while preserving its modular character, the tools were enhanced to support streaming of slices of md-arrays.

2.2 Slicing

Suppose for $n \in \mathbb{N}$ that we want to split up an n -dimensional array $X \in \mathbb{C}^{N_0 \times N_1 \times \dots \times N_{n-1}}$. In the following, the entries $X_{(i_0, \dots, i_{n-1})}$ of X are referenced using the multi-index

$$(i_0, \dots, i_{n-1}), \quad i_j \in \mathbb{N}_0 \text{ and } i_j < N_j - 1.$$

One method to subdivide this array is slicing i. e. to select a set of axes, and take those subsets of the array within which the indices of the selected axes stay constant. This concept is illustrated in Figure 1A. To give a precise description, if $A := \{0, 1, \dots, n-1\}$ is the set of all axes of the array, then, for some $m < n$, $m \in \mathbb{N}$, a subset of m axes $S \subset A$ is first selected for slicing. Any given multi-index can then be decomposed into two multi-indices a and b :

$$(i_{S(0)}, \dots, i_{S(m-1)}) = (a_0, \dots, a_{m-1}), \quad (1)$$

$$(i_{F(0)}, \dots, i_{F(n-m-1)}) = (b_0, \dots, b_{n-m-1}), \quad (2)$$

where $F = A \setminus S$ is the set of free axes, and $S(k)$ and $F(k)$ denote the k -th smallest entry of the set S and F , respectively. In other words, X is split into a number of $n - m$ dimensional sub-arrays or “slices” by fixing part of the multi-index in every slice.

Every slice is associated with one specific multi-index a . The set of all slices can be enumerated by flattening the multi-index a into a serial number, i.e. a single integer

$$c = \sum_{k=0}^{m-1} a_k \left(\prod_{l=0}^{k-1} N_{S(l)} \right). \quad (3)$$

As common in BART, the selected set of dimensions S used for this slicing operation can be efficiently encoded as a single integer using a bitmask. This is done by interpreting the pattern of selected/non-selected axes as a binary number

$$\text{bitmask}(S) = \sum_{i \in S} 2^i. \quad (4)$$

2.3 Looping

The idea of looping is to apply the functionality of a BART tool sequentially to every slice, instead of applying it once to the whole array (normal/*combined* operation). The invoked BART tool then does not “see” the entire array, but instead operates on a single slice. This can sometimes lead to semantic differences, e.g. when a full 3D reconstruction is numerically different to reconstruction decoupled into slices. In many cases, looping will lead to exactly the same result, but modifies computing requirements and applicability: e.g. reducing memory requirements, or enabling distribution across high-performance cluster or multiple GPUs.

The looping functionality in BART is controlled using a newly added set of options, referred to as *loop options*, which are passed to the `bart` driver command. More information on loop options can be found in the BART help, accessible by calling `bart -h`, and the documentation folder of the BART repository. Figure 1B illustrates looping in a self-contained example.

2.4 Streaming

The goal of BART's streaming feature is to enable pipeline processing by letting the tools send and receive slices of md-arrays during the computation. This enables a chain of tools to simultaneously process different slices as part of a single reconstruction pipeline.

BART will use streaming automatically based on the file name of the argument. First, streaming is active if a hyphen is specified as file name, which by convention is understood as a reference to standard input/output. Using the vertical-bar or pipe operator `|` available in common shells on UNIX-derived systems [38], a series of BART commands can be started in parallel, such that the standard output of one command is connected to the standard input of the next command. Second, BART uses streaming when a file name ends in `.fifo`. *Fifos* (First-In-First-Out-Files / named pipes) enable streaming of multiple in-/outputs at the same time, which is needed to write complex reconstruction scripts with streaming support, as described later in Section 2.5.

Generally, all BART tools directly support streaming. By default, a tool will wait (block) until all data in a stream has fully arrived. This is essentially the same behavior that would also occur if no streams were used. A more powerful method is to combine streaming and looping. If a specified reference file is a stream, the stream flags are directly used as loop flags and the BART tool is invoked on every slice as soon as it is received. Thus, the combination of the loop functionality and streaming allows any BART tool to be used as part of a pipeline without blocking it. Additionally, several tools have been made stream-aware, to simplify certain operations such as regularization onto previous frames in real-time applications of `nlinv`.

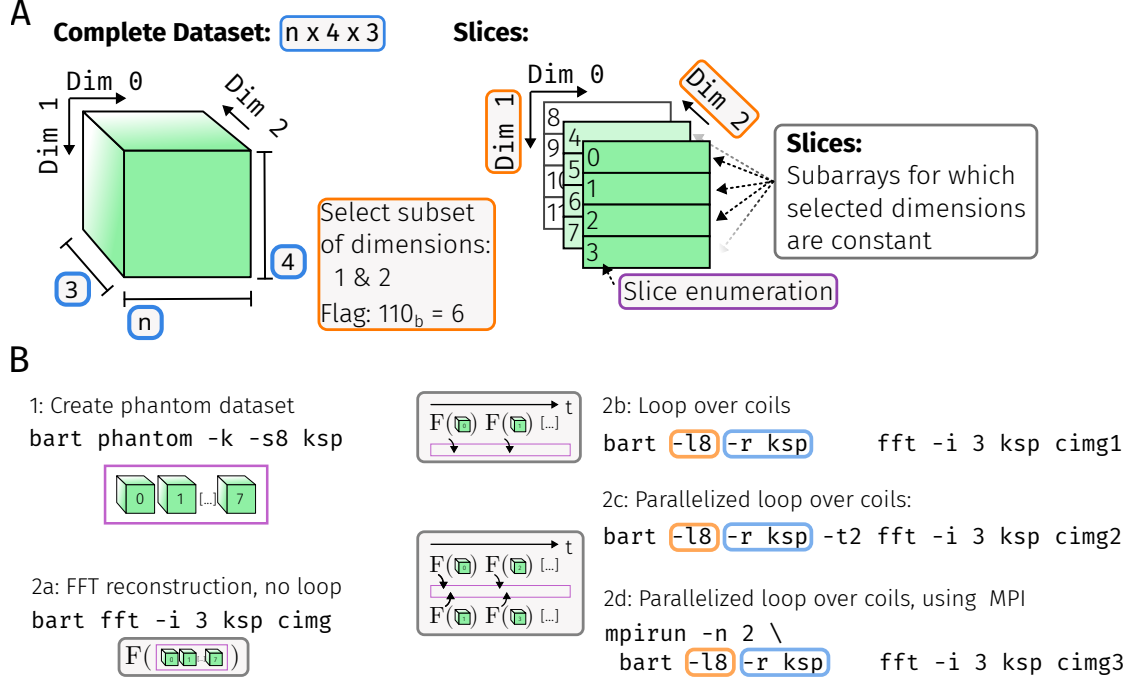


Figure 1: A: Schematic of how a three-dimensional array can be sliced. The cube on the left symbolizes the full three-dimensional array. By selecting a set of dimensions $\{2, 1\} \subset \{2, 1, 0\}$, the array can be decomposed into a set of slices for which the index along dimension 0 stays constant, as shown on the right. The set of selected axes can be efficiently encoded as a bitmask $6 = 1 \times 2^2 + 1 \times 2^1 + 0 \times 2^0$ (Equation (4)), and every slice is uniquely identified through a serial number.

B: Example command lines which demonstrate how slicing can be used in BART. First, a k-space dataset with multiple channels is generated using command 1. Commands 2a-d then calculate the FFT of it by using the `fft-tool` in different ways: Command 2a processes the dataset in a single invocation (*combined*). Command 2b processes all channels serially. This is specified using the loop option `-l 8`, where $8 = 2^3$ represents the coil sensitivity dimension, and the reference file `-r ksp` provides the loop limits. Command 2c uses the `-t` (threads) option to process all channels in parallel in two threads. Note that 2a will typically use multiple threads as well, but on a lower level within the FFT implementation itself. Finally, 2d uses `mpirun` to process the dataset on two nodes [36] or two GPUs.

2.5 Applications

We demonstrate the application of BART streams in three different exemplary scenarios: a gridding reconstruction, a complete RT-NLINV reconstruction with preprocessing, and a comprehensive reconstruction script accomodating various steps for advanced RT-MRI.

To begin, reconstruction for RT-MRI using radial sampling can be performed using the adjoint non-uniform FFT (NUFFT) or *gridding* [39]. Here, the raw k-space data from the scanner is first multiplied with the Ram-Lak filter [40], to compensate for non-uniform sampling density of radial sampling. Afterwards, the adjoint NUFFT is applied to obtain coil images, which are combined using root sum-of-squares. Compared to iterative reconstructions, this scheme is relatively simple and can run in real-time even without GPU acceleration. Figure 2A shows an RT-MRI pipeline implementation of this reconstruction using BART streams.

Figure 2B shows a more sophisticated reconstruction using RT-NLINV, which however still requires only a few BART commands. Here, we also employ a new dynamic variant of geometric coil compression [35] which is adapted to RT-MRI by performing alignment of the compression matrices along the time dimension [41]. Using this method requires incoming data to be split up, processed, and then recombined in real-time.

As a final example, a complete state-of-the-art reconstruction pipeline for radial real-time MRI was created. It takes the form of a BASH script which launches different reconstruction pipelines, based either on the gridding-based reconstruction (Figure 2A) combined with a sliding window strategy [42], or on RT-NLINV. Additional preprocessing steps such as coil compression and gradient delay correction based on RING [43] and post processing steps such as a median filter or non-local means filter [44] can be selected by the user. A graph representation of one reconstruction pipeline generated by this script is available in supporting material S1.

2.6 MRI Scans

We show exemplary results of the real-time reconstruction script on cardiac scans of a healthy adult volunteer, who was examined with approval by the local ethics board and after giving written informed consent. As this work mainly focusses on technical implementation, our findings are largely independent of subject variability, and should generalize well. Measurements were done with a Magnetom Vida 3T (Siemens Healthineers, Erlangen, Germany) using a radial FLASH [45] sequence with random RF-spoiling [46] and a turn-based pattern with 5 turns and 13 spokes per turn [42]. Further parameters are given in Table 1. In addition, phantom scans were performed to measure end-to-end latency as described in [47], cf. supporting material Figure S2.

All images shown are reconstructed using the real-time reconstruction script introduced in Section 2.5. We compare images from different quality settings:

- *Fast*: Gridding-based reconstruction, with static coil compression to four channels.
- *Good*: Gradient delay correction, coil compression to eight channels, RT-NLINV-reconstruction and five-frame median-filtering

Table 1: Parameters of the RF-spoiled radial FLASH MRI measurements.

Parameter	Value
ADC Samples ($2 \times$ oversampling)	256
Spokes / frame	13
Matrix size	192
Flip angle	10°
TR	2.1 ms
TE	1.25 ms
FOV	256 mm
Bandwidth	1300 Hz pixel ⁻¹
Slice thickness	5 mm

- *High*: Gradient delay correction, aligned coil compression to eight channels, RT-NLINV reconstruction with more iterations, median filtering and additional non-local means filtering [44].

Good and *High* quality reconstructions were accelerated using an Nvidia H100 GPU (80 GB HBM3, SXM) on a system with an AMD EPYC 9334 CPU. *Fast* quality reconstruction is done without GPU acceleration.

Additionally, we assess the impact of aligned dynamic coil compression as described in Section 2.5. This is based on the *good* quality setting, but omitting any post-processing steps. We compare the following choices for coil compression (CC): Static CC using data from the first frame, static CC using data from all frames (non-causal), dynamic CC on every frame separately, and aligned dynamic CC.

Reconstructions are run on a server in the neighbouring building, connected to the acquisition system via 1 Gigabit Ethernet. Data is exchanged with the MRI scanner using BART streams with a custom data import/export software that is integrated into the vendor software (ICE) running on the scanner, which sends out every k-space line over the network as soon as it was acquired. Conversely, every received image is forwarded to ICE for display as soon as it is received.

2.7 Latency and Performance Measurements

Computational performance of the new BART features was evaluated. With only a single thread on one compute node, looping will typically be slower than combined operation due to overhead such as repeated initialization. We first quantify this overhead imposed by streaming/looping. Furthermore, we measure the peak amount of memory which was simultaneously used by BART in the computer’s main memory (resident set size).

First, an md-array of complex random numbers $\mathbf{x} \in \mathbb{C}^{n_r \times n_p \times n_s}$ is created, representing raw data from a Cartesian multi-slice MRI measurement for different matrix sizes n_r , n_p with oversampling in readout direction $n_r = 2n_p$ and a varying number of slices n_s . An inverse 2D-FFT of every slice is then performed in three different ways (cf. Fig-

ure 1). First, with a regular BART command, resulting in combined processing of the data:

```
bart fft -i 3 x out
```

Second, the 2D-FFT is sequentially performed on every slice using the loop options:

```
bart -l4 -r x fft -i 3 x out
```

Third, data is read by the looped `fft` command from a previously created text file using the stream protocol:

```
bart -l4 -r x copy x - > stream.txt
bart -l4 -r - fft -i 3 - out < stream.txt
```

In a second experiment, we measure the speed-up for a simple reconstruction pipeline where streaming and looping enable parallelization of consecutive reconstruction steps. A customizable delay is added to the input stream, simulating per-slice acquisition time. The output of the `copy-tool` is then forwarded to the `fft-tool` directly via a pipe, causing the processes to run in parallel:

```
bart -l4 -r x copy --delay <delay> x - |\
bart -l4 -r - fft -i 3 - out
```

This is compared to the static variant:

```
bart -l4 -r x copy --delay <delay> x - |\
bart fft -i 3 - out
```

where the reconstruction can only begin after the `copy`-process has processed all slices. The experiment is repeated for different delays between 0 ms and 130 ms. Wall-clock run time is measured using the `date` program from GNU Coreutils. The experiments were repeated 25 times to measure standard deviation across runs, and performed on a standard workstation using an Intel Xeon W-2123 CPU running at 3.60 GHz.

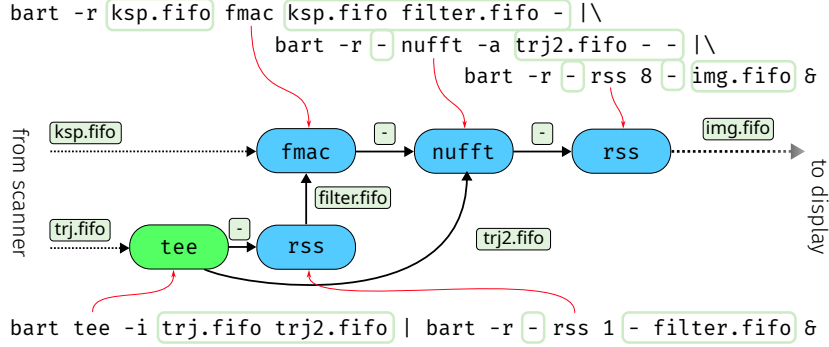
To assess latency for real-time MRI, phantom measurements were performed. We use the real-time reconstruction script (Section 2.6, set to *good*), and additionally run the experiment without median filter to assess the impact of this post-processing step on overall latency. Apart from acquisition and the reconstruction, several other factors such as network transfer times, filters used in post processing, and image display are expected to contribute to the total latency. Therefore, we determined several different latencies:

- Latency in BART is calculated as time difference between arrival of the last spoke and transmission of the reconstructed frame. Preprocessing, reconstruction and post processing were also measured individually. Timestamps are recorded using the `gettimeofday` function from `glibc`.
- Latency BART + Network as seen from the software running on the scanner is measured by taking timestamps when the last spoke is sent over the network and

after the corresponding frame has been received. This also includes data transfer times and network delays.

- End-to-end latency, i. e. the time between an event happening in the scanner until it is shown on the MRI screen, is measured using an experimental setup as described in [47] , correlating movements in a phantom with movement on the screen using a video recording. Additional information is available in supporting material S2.

Because the MRI acquisition starts as soon as possible without waiting for the BART reconstruction pipeline to be initialized, the latency decreases towards a steady state, which is reported here as *steady state latency*.

A: Gridding Reconstruction**B: NLINV Reconstruction with Dynamic Coil Compression**

```

SIZE=128 OS=2 OS_SIZE=$((SIZE * OS))
bart tee -i ksp.fifo ksp_tmp.fifo | bart -r - cc -M - - | \
    bart ccapply -A 10 -p 6 ksp_tmp.fifo - - | \
    bart nlinv -x $OS_SIZE:$OS_SIZE:1 \
        --real-time -t trj_s.fifo - - | \
    bart -r - resize -c 0 $SIZE 1 $SIZE - img.fifo &
    bart -r trj.fifo scale $OS trj.fifo trj_s.fifo &

```

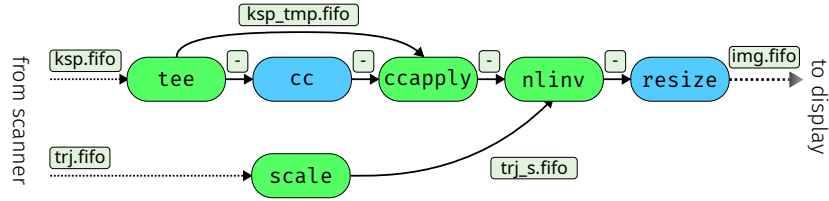


Figure 2: Part **A** shows a simple reconstruction pipeline using a Ram-Lak filter, an adjoint NUFFT, and root sum-of-squares coil combination. Shell code with which the pipeline can be created is shown along with a representation of the computational graph. Edges represent files, large colored nodes represent BART processes. `ksp.fifo` and `trj.fifo` are named pipes, which are expected to deliver incoming k-space data and trajectory from the scanner or previous processing steps. Similarly, `img.fifo` provides reconstructed images for further processing and display. Colors in the process nodes are used to highlight how tools can utilize streams in different ways. Blue commands use the loop options, while green commands are stream-aware.

Part **B** shows an example for an advanced reconstruction where geometric coil compression and NLINV are used for real-time reconstruction of radial data. Incoming raw data is first split with the `tee` command and forwarded to two different tools, `cc` and `ccapply`. The `cc` tool calculates the coil compression matrices, but does not apply them. Instead, they are forwarded to the `ccapply` tool, which applies the received matrices to the incoming raw data and forwards the compressed k-space to the `nlinv` reconstruction. A subsequent `resize` command removes oversampling in the image domain.

3 Results

3.1 Performance

3.1.1 Numerical experiments

We first present results on the performance of the two main additions to the BART software, streaming and looping. As described in Section 2.7, looping and streaming can under some conditions create computational overhead. Figure 3A shows the overhead when performing a looped FFT compared to normal FFT. For small arrays with many iterations / slices, there is a large relative overhead. E.g., the FFT of a 96x48x100 array takes 50% or 10(1) ms (mean with standard deviation in parentheses) longer when looping over the last dimension. FFT of a 2048x1024x100 array takes 2% or 400(150) ms longer. For few slices or large problem sizes, the differences between looping and combined operation are small relative to the variation over repetitions.

In Figure 3B, we repeat this analysis for the streaming protocol, comparing the extra time required when performing looping with a streamed input as opposed to looping alone. The maximum overhead is several times smaller than in the previous analysis. Furthermore, the overhead induced by the stream protocol is smaller than the average run-to-run variation in most cases. Also, there is no clear trend towards any greater or smaller overhead depending on the matrix size.

Figure 3C, illustrates how, with looping, peak memory usage is independent of the number of slices while it grows linearly with normal i.e. combined operation. Furthermore, combined streaming and looping enables parallelization of successive data processing steps, and thus can speed up computation. This is illustrated in Figure 3D. Depending on matrix size and delay (slice acquisition time), total elapsed time was reduced down to a minimum of 56% of the reference.

3.1.2 End-to-End Latency

The latency of our RT-MRI setup was measured using different methods (Section 2.7). The measurement was repeated three times, with almost identical outcome. One instance of these measurements is shown in Figure 4. The BART-internal timing measurements reveal the amounts of time required for preprocessing, reconstruction and post processing, which are 3(2) ms, 13(2) ms and 13(1) ms, respectively. Relative to the acquisition time of a single frame, which is $13 \cdot 2.1 \text{ ms} = 27.3 \text{ ms}$, all steps are relatively fast. Without the median filter post processing time is 2(1) ms.

The latency measured from the perspective of the software running on the scanner matches the total latency measured within BART with a difference of approximately 5 ms corresponding to the network transfer. The end-to-end latency of 205(20) ms is several times larger than the other two latency measurements with only 28(2) ms from the BART reconstruction. This discrepancy between end-to-end latency compared to the other measurements has multiple sources. For instance, the acquisition time itself contributes to the end-to-end latency. Furthermore, time-dependent filters such as the median filter do not affect the signal processing time too much, but have a large impact

on the end-to-end latency. Without median filter, an end-to-end latency of 146(13) ms is achieved. Several other possible sources are treated in the discussion.

3.2 Real-Time Applications

In our experimental setup, the simple reconstruction based on the adjoint NUFFT can be run in real-time on standard hardware without use of a GPU as demonstrated by the latency graph shown in Figure 5E. Iterative reconstruction methods such as RT-NLINV can be used to achieve high image quality, which can be further improved through post processing, as seen in Figure 5B-D. The initially higher, but then quickly decreasing latency in these cases is probably due to initialization of the GPU and precomputing steps. A comparison between non-causal reconstruction and real-time capable reconstruction can be found in the literature [20]. Videos of the reconstruction are available in supporting material S3.

Figure 6 compares static and dynamic coil compression and demonstrate the impact of aligned dynamic coil compression as described in Section 2.5. In Figure 6A, it can be seen that noise is increased after a change of slice position, as the compression matrix is not adapted to the changed coil profiles in the new slice. Dynamic coil compression leads to problems as shown in Figure 6B: The coil profiles show distinct jumps over their time course and this then also affects the reconstructed images. These discontinuities disappear when using aligned dynamic coil compression. For comparison, we also show coil and image profiles from reconstruction with static coil compression, which exhibit no discontinuities/brightness jumps.

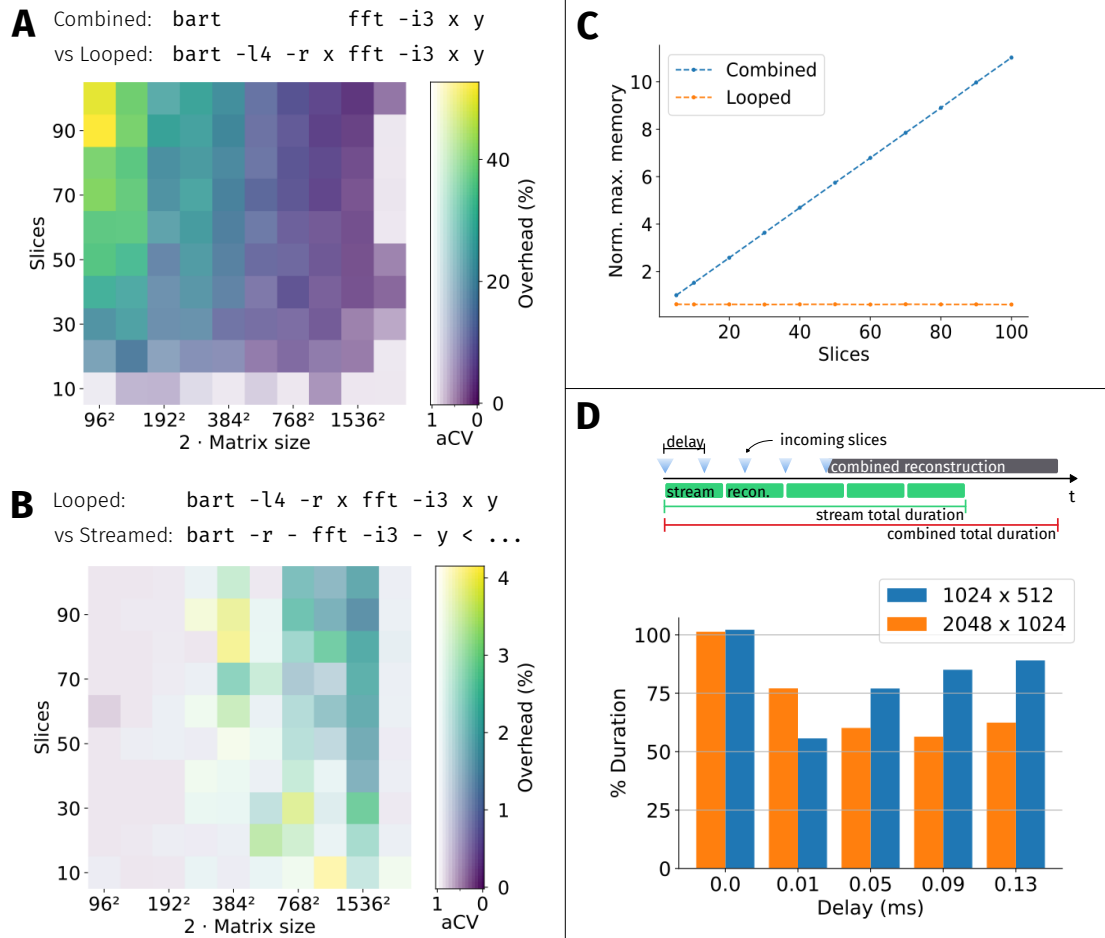


Figure 3: The performance of BART looping and streaming is shown here by visualizing the runtime of an inverse FFT on arrays of varying size.

Part **A** shows a heat map of additional time required when performing a looped FFT relative to the normal/combined FFT, for different problem sizes. The opacity/lightness is based on an adjusted coefficient of variation (aCV): Fully saturated colors represent a distinct overhead, while light colors indicate that the average run-to-run difference is at least as big as the calculated overhead.

Part **B** compares the overhead of streaming relative to looping, similar to part A.

Part **C** visualizes the memory advantage of looped versus combined operation for a matrix size of 512×256 with varying number of slices. Memory usage is normalized to the amount required for a single slice, i. e. array size $512 \times 256 \times 1$.

Part **D** shows the speed-up due to reduced waiting times in pipeline operation, i. e. when the process producing the data (acquisition) and the reconstruction can be parallelized.

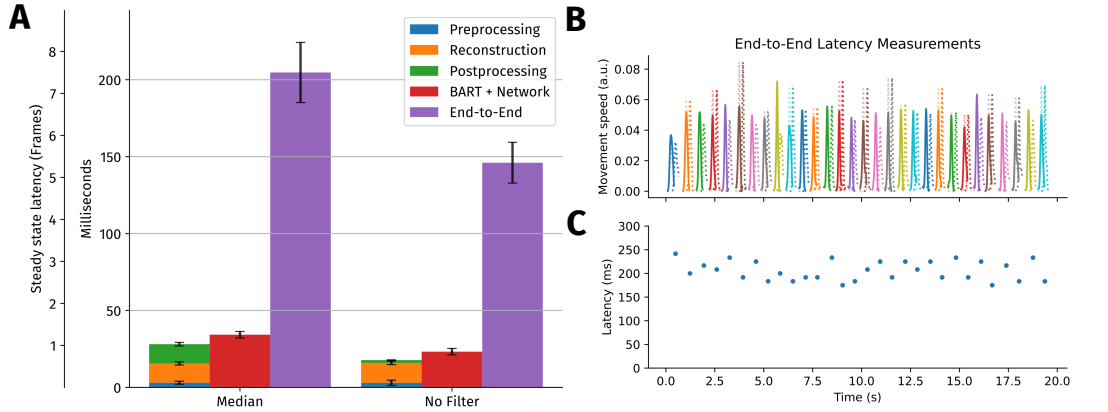


Figure 4: Latency measurements for RT-MRI. Part **A** visualizes results from three different latency measurement methods described previously. Latency determined within BART is further separated into three different steps: preprocessing, reconstruction and post processing. The times are shown for two measurements, with and without median filter in the post processing chain. Error bars indicate standard deviation over the course of the time series. An initially higher end-to-end latency in the first few seconds is excluded for calculating the steady-state end-to-end latency shown here.

Part **B** on the right highlight details of the end-to-end latency measurement. Every colored line corresponds to a movement in the end-to-end latency measurement setup. Solid lines are calculated from the optically observed movement, while dashed lines correspond to the movement observed in the reconstructed images shown on the MRI console. The optimally shifted MRI movement curves are shown with transparent dashed lines. In **C**, the resulting time series of end-to-end latency measurements is shown.

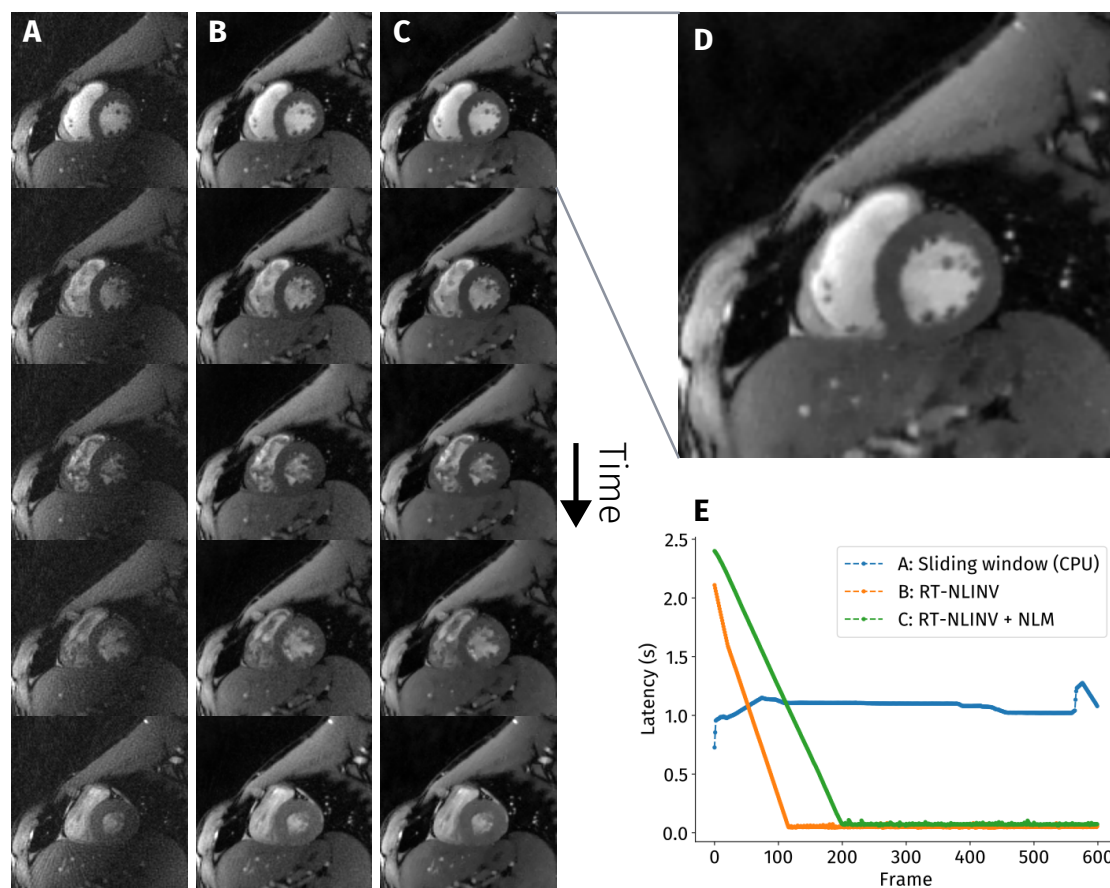


Figure 5: Five representative frames covering one heartbeat from a real-time acquisition of a cardiac short-axis view, reconstructed with different quality settings for the real-time reconstruction script (Section 2.6). Column **A** shows images reconstructed with *fast*, column **B** *good* and column **C** *high* quality settings. Part **D** provides an enlarged view of the *high* quality setting. The graph **E** shows the numerically determined latency of all configurations.

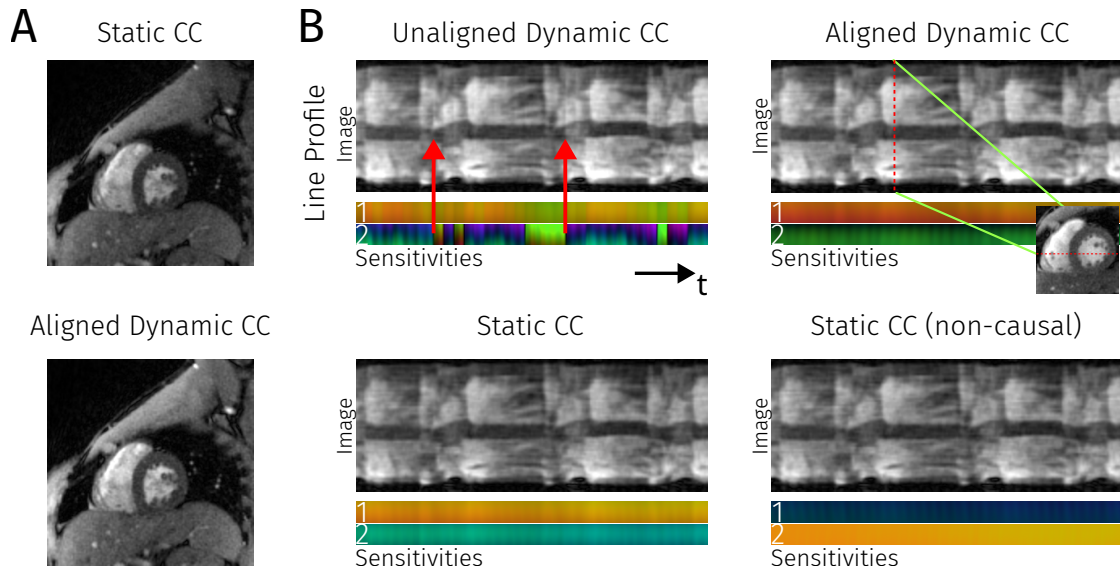


Figure 6: Part **A** compares two frames from a RT-MRI of the heart with different strategies for coil compression, either re-using the compressing matrix or recomputing and aligning it for every frame. The red arrows highlight abrupt changes in image magnitude which correlate with the discontinuities in the virtual coil profiles. Part **B** shows a time series from a line through the heart, with the line being shown in the small inset image. The bottom row shows the time series for the first two virtual coil profiles, the top row shows the actual images. On the top left, every frame was independently compressed, on the top right, compression matrices were aligned using geometric coil compression. For comparison, line profiles for coil compression done on the first frame/complete dataset are shown in the bottom left/right.

4 Discussion

Streaming functionality was added to the BART reconstruction software as new feature. The implementation achieves high modularity and interoperability for real-time reconstruction pipelines by relying on standard operating system utilities. Based on a set of new options, all tools included in the toolbox can be used in real-time reconstruction pipelines.

The streaming extension was tested and benchmarked in numerical experiments and using phantom and in-vivo measurements. As it is now possible to parallelize subsequent reconstruction steps in a pipeline, a speed-up can be achieved for conventional reconstruction pipelines simply by chaining BART commands. Under certain circumstances, the overhead associated with streaming and looping can have a negative effect on performance, but in all tested conditions overhead was either small in absolute units, small compared to the total computation time, or small relative to the run-to-run variations. In most practical applications, the overhead should not be relevant or even be unnoticeable.

Naturally, there is some overlap between BART and other reconstruction frameworks, such as the Gadgetron [31] and also with vendor pipelines. Nevertheless, BART is not meant to replace such other frameworks, but to provide a set of versatile tools that can be used to solve specific problems in a variety of scenarios. In fact, it is very common to only use specific BART tools as part of other projects and this is facilitated by BART's open and modular design. So far, this was exploited mostly for offline reconstruction. By providing a low-latency path for continuous data exchange, BART can now also be integrated into real-time processing pipelines.

To demonstrate the flexibility of the new streaming framework, we showed examples that extend from simple NUFFT-based reconstruction which can be used even on desktop systems to advanced iterative reconstruction that achieves image quality and makes use of GPU acceleration. The advantages of dynamic coil compression was shown, demonstrating how advanced functionality can be implemented in a modular pipeline. We provide a versatile reconstruction script for real-time as part of the BART toolbox that includes all the functionality described in this work. New BART functionality such as removal of phase pole artefacts [48] were also already integrated and shown to be beneficial in preliminary experiments.

We furthermore measured the latency of our interactive RT-MRI setup for a full reconstruction pipeline. Here, we found that the part of the latency corresponding to the BART pipeline is only a small fraction of the overall end-to-end latency. Processing time in BART, including network transfer, is below 30 ms, which is acceptable even for demanding application such as cardiac interventional MRI. End-to-End latency is considerably higher with 200 ms, which is in part explained by the response of the median filter used in post processing, and the duration of the data acquisition itself. As shown previously [49] the temporal regularization does not add substantial latency. Another source of end-to-end latency is image processing in the vendor software, which includes e. g. distortion correction and displaying of the images.

For integration with the MRI scanner, we used a custom, vendor-specific software for data import/export. However, we also already performed initial experiments using scanner integration based on MRD streams, using the BART `ismrmd` tool to interface at the start/end of the reconstruction pipeline. With vendors increasingly providing open interfaces, this should simplify the integration of BART into custom pipelines.

5 Conclusion

The streaming extension to the BART framework enables efficient reconstruction for RT-MRI applications with low latency, while retaining the full modularity of the BART framework.

Conflict of Interest

The authors declare no competing interests.

Data Availability Statement

In the spirit of reproducible research, the code to reproduce the results of this paper is available at <https://gitlab.tugraz.at/ibi/mrirecon/papers/bart-streams> (version v0.2). All reconstructions have been performed with BART, available at <https://github.com/mrirecon/bart> and <https://codeberg.org/mrirecon/bart>. The data used in this study is available at Zenodo 10.5281/zenodo.17671124.

The authors are committed to supporting BART for at least another ten years. Long-term reproducibility is ensured by regular automated testing. A mailing list is available for questions and problems can be reported via a publicly available contacts. Code contributions are welcomed.

Acknowledgements

This work was funded by DZHK (German Centre for Cardiovascular Research) grant 81X4300119 and in part by NIH under grant U24EB029240.

The authors thank the ISMRM Reproducible Research Study Group for conducting a code review of the code (Version v0.1) supplied in the Data Availability Statement. The scope of the code review covered only the code's ease of download, quality of documentation, and ability to run, but did not consider scientific accuracy or code efficiency.

References

- [1] Riederer SJ, Tasciyan T, Farzaneh F, Lee JN, Wright RC, Herfkens RJ. MR fluoroscopy: Technical feasibility. *Magn. Reson. Med.* 1988; 8:1–15.

-
- [2] Nayak KS. Response to Letter to the Editor: “Nomenclature for real-time magnetic resonance imaging”. *Magn. Reson. Med.* 2019; 82:525–526.
- [3] Dietz B, Fallone BG, Wachowicz K. Nomenclature for real-time magnetic resonance imaging. *Magn. Reson. Med.* 2019; 81:1483–1484.
- [4] Buecker A, Neuerburg JM, Adam GB, et al. Real-time MR fluoroscopy for MR-guided iliac artery stent placement. *Journal of Magnetic Resonance Imaging* 2000; 12:616–622.
- [5] Ratnayaka K, Faranesh AZ, Hansen MS, et al. Real-time MRI-guided right heart catheterization in adults using passive catheters. *Eur. Heart J.* 2013; 34:380–389.
- [6] Campbell-Washburn AE, Faranesh AZ, Lederman RJ, Hansen MS. Magnetic resonance sequences and rapid acquisition for MR-guided interventions. *Magn. Reson. Imaging Clin. N.* 2015; 23:669–679.
- [7] Unterberg-Buchwald C, Ritter CO, Reupke V, et al. Targeted endomyocardial biopsy guided by real-time cardiovascular magnetic resonance. *J. Cardiovasc. Magn. Reson.* 2017; 19:45.
- [8] Nageotte SJ, Lederman RJ, Ratnayaka K. MRI Catheterization: Ready for Broad Adoption. *Pediatric Cardiology* 2020; 41:503–513.
- [9] Neves Silva S, Aviles Verdera J, Tomi-Tricot R, et al. Real-time fetal brain tracking for functional fetal MRI. *Magn. Reson. Med.* 2023; 90:2306–2320.
- [10] Nayak KS, Pauly JM, Nishimura DG, Hu BS. Rapid ventricular assessment using real-time interactive multislice MRI. *Magn. Reson. Med.* 2001; 45:371–375.
- [11] Narayanan S, Nayak K, Lee S, Sethy A, Byrd D. An approach to real-time magnetic resonance imaging for speech production. *J. Acoust. Soc. Am.* 2004; 115:1771–1776.
- [12] Niebergall A, Zhang S, Kunay E, et al. Real-time MRI of speaking at a resolution of 33 ms: Undersampled radial FLASH with nonlinear inverse reconstruction. *Magn. Reson. Med.* 2013; 69:477–485.
- [13] Rasche V, Boer RWD, Holz D, Proksa R. Continuous radial data acquisition for dynamic MRI. *Magn. Reson. Med.* 1995; 34:754–761.
- [14] Saybasili H, Herzka DA, Seiberlich N, Griswold MA. Real-time imaging with radial GRAPPA: Implementation on a heterogeneous architecture for low-latency reconstructions. *Magn. Reson. Imag.* 2014; 32:747–758.
- [15] Lustig M, Donoho D, Pauly JM. Sparse MRI: The application of compressed sensing for rapid MR imaging. *Magn. Reson. Med.* 2007; 58:1182–1195.
- [16] Majumdar A, Ward RK, Aboulnasr T. Compressed Sensing Based Real-Time Dynamic MRI Reconstruction. *IEEE Transactions on Medical Imaging* 2012; 31:2253–2266.
- [17] Sumbul U, Santos J, Pauly J. A Practical Acceleration Algorithm for Real-Time Imaging. *IEEE Transactions on Medical Imaging* 2009; 28:2042–2051.

- [18] Le DH, Kumar P, Yagiz E, Tian Y, Nayak KS. Online Spatiotemporally Constrained Reconstruction for Real-Time Interactive MRI. *Magn. Reson. Med.* 2025; 95:1644–1652.
- [19] Uecker M, Zhang S, Voit D, Karaus A, Merboldt KD, Frahm J. Real-time MRI at a resolution of 20 ms. *NMR Biomed.* 2010; 23:986–994.
- [20] Uecker M, Zhang S, Frahm J. Nonlinear inverse reconstruction for real-time MRI of the human heart using undersampled radial FLASH. *Magn. Reson. Med.* 2010; 63:1456–1462.
- [21] Uecker M, Hohage T, Block KT, Frahm J. Image reconstruction by regularized nonlinear inversion-joint estimation of coil sensitivities and image content. *Magn. Reson. Med.* 2008; 60:674–682.
- [22] Nayak KS, Lim Y, Campbell-Washburn AE, Steeden J. Real-Time Magnetic Resonance Imaging. *J. Magn. Reson. Imaging* 2022; 55:81–99.
- [23] Sorensen TS, Atkinson D, Schaeffter T, Hansen MS. Real-time reconstruction of sensitivity encoded radial magnetic resonance imaging using a graphics processing unit. *IEEE Trans. Med. Imag.* 2009; 28:1974–1985.
- [24] Schaetz S, Uecker M. A multi-GPU programming library for real-time applications. In: *Int. Conf. Alg. Arch. Parallel Process.* Vol. 12. Fukuoka; 2012:114–128.
- [25] Green OL, Rankine LJ, Cai B, et al. First clinical implementation of real-time, real anatomy tracking and radiation beam control. *Medical Physics* 2018; 45:3728–3740.
- [26] Kumar P, Tian Y, Lim Y, et al. State-of-the-art speech production MRI protocol for new 0.55 Tesla scanners. In: ISCA. ISCA; 2024.
- [27] Blumenthal M, Heide M, Holme C, et al. *Mrirecon/Bart: Version 0.9.00*. Zenodo. 2023. doi: 10.5281/ZENODO.592960.
- [28] Uecker M, Lai P, Murphy MJ, et al. ESPIRiT—an eigenvalue approach to autocalibrating parallel MRI: where SENSE meets GRAPPA. *Magn. Reson. Med.* 2014; 71:990–1001.
- [29] Blumenthal M, Luo G, Schilling M, Holme HCM, Uecker M. Deep, deep learning with BART. *Magn. Reson. Med.* 2023; 89:678–693.
- [30] Blumenthal M, Fantinato C, Unterberg-Buchwald C, Haltmeier M, Wang X, Uecker M. Self-supervised learning for improved calibrationless radial MRI with NLINNet. *Magn. Reson. Med.* 2024. doi: 10.1002/mrm.30234.
- [31] Hansen MS, Sørensen TS. Gadgetron: An open source framework for medical image reconstruction. *Magn. Reson. Med.* 2013; 69:1768–1776.
- [32] Inati SJ, Naegele JD, Zwart NR, et al. ISMRM Raw data format: A proposed standard for MRI raw datasets. *Magn. Reson. Med.* 2016; 77:411–421.
- [33] Diakite M, Campbell-Washburn AE, Xue H. Integration of the BART Toolbox into Gadgetron Streaming Framework for Inline Cloud-Based Reconstruction. In: *Proc. Intl. Soc. Mag. Reson. Med.* Vol. 26. Paris; 2018:2861.

- [34] Veldmann M, Ehses P, Chow K, Nielsen JF, Zaitsev M, Stöcker T. Open-source MR imaging and reconstruction workflow. *Magn. Reson. Med.* 2022; 88:2395–2407.
- [35] Zhang T, Pauly JM, Vasanawala SS, Lustig M. Coil compression for accelerated imaging with Cartesian sampling. *Magn. Reson. Med.* 2013; 69:571–582.
- [36] Message Passing Interface Forum. *MPI: A Message-Passing Interface Standard Version 4.1*. 2023. URL: <https://www.mpi-forum.org/docs/mpi-4.1/mpi41-report.pdf>.
- [37] Blumenthal M, Uecker M. Large-Scale High-Dimensional Image Reconstruction Via Delayed And Distributed Computing With BART. In: *Proc. Intl. Soc. Mag. Reson. Med.* 2025:1281.
- [38] Ritchie DM. The Evolution of the UNIX Time-sharing System. *AT & T Bell Laboratories Technical Journal* 1984; 63:1577–1593.
- [39] O’Sullivan JD. A fast sinc function gridding algorithm for Fourier inversion in computer tomography. *IEEE Trans. Med. Imag.* 1985; 4:200–207.
- [40] Ramachandran G, Lakshminarayanan A. Three-dimensional reconstruction from radiographs and electron micrographs: application of convolutions instead of Fourier transforms. *PNAS* 1971; 68:2236–2240.
- [41] Schaten P, Blumenthal M, Rapp B, Uecker M. BART streams: a plug & play framework for interactive real-time MRI at the example of aligned dynamic coil compression. In: *Book of Abstracts ESMRMB 2024 Online 40th Annual Scientific Meeting*. 2024:719–721.
- [42] Zhang S, Block KT, Frahm J. Magnetic resonance imaging in real time: advances using radial FLASH. *J. Magn. Reson. Imaging* 2010; 31:101–109.
- [43] Rosenzweig S, Holme HCM, Uecker M. Simple auto-calibrated gradient delay estimation from few spokes using Radial Intersections (RING). *Magn. Reson. Med.* 2019; 81:1898–1906.
- [44] Buades A, Coll B, Morel JM. A Non-Local Algorithm for Image Denoising. In: *2005 IEEE Computer Society Conference on Computer Vision and Pattern Recognition (CVPR)*. Vol. 2. 2005:60–65.
- [45] Haase A, Frahm J, Matthaei D, Hanicke W, Merboldt KD. FLASH imaging. Rapid NMR imaging using low flip-angle pulses. *J. Magn. Reson.* 1986; 67:258–266.
- [46] Roeloffs V, Voit D, Frahm J. Spoiling without additional gradients: Radial FLASH MRI with randomized radiofrequency phases. *Magn. Reson. Med.* 2016; 75:2094–2099.
- [47] Schaten P, Blumenthal M, Uecker M. BART Streams: End-to-End Latency of Real-Time MRI. In: *Book of Abstracts ESMRMB 2025 Online 41st Annual Scientific Meeting*. 2025:496–497.
- [48] Blumenthal M, Uecker M. *Phase-Pole-Free Images and Smooth Coil Sensitivity Maps by Regularized Nonlinear Inversion*. 2025. arXiv: 2508.04685.

- [49] Frahm J, Schätz S, Untenberger M, et al. On the Temporal Fidelity of Nonlinear Inverse Reconstructions for Real- Time MRI – The Motion Challenge. *The Open Medical Imaging Journal* 2014; 8:1–7.
- [50] Gansner ER, North SC. An open graph visualization system and its applications to software engineering. *Software: Practice and Experience* 2000; 30:1203–1233.

Supporting Information

List of supporting material, including captions.

S1 Real-Time MRI Reconstruction Pipeline Graph

Figure S1: State-of-the-art reconstruction pipeline for real-time MRI. Different sections of the reconstruction pipeline are highlighted, and characteristic parts are also shown in a zoomed-in, abbreviated version next to the full graph. Round nodes represent BART invocations while edges between tool nodes represent pipes. The invocation of the real-time reconstruction script corresponding to this graph is shown at the bottom, along with an explanation of command line options. The figure is based on an auto-generated graph, which was created by tracing every BART tool invocation and translating this trace into a graph description language, and was rendered with `dot` [50].

S2 End-To-End Latency Measurement

Figure S2: Part **A**: Schematic overview of the end-to-end latency measurement experiment setup. A water-filled test-tube (blue) inside the MRI scanner is pulled up from the control room using a long string (yellow). Images from the real-time sequence are shown on the MRI console screen. A smartphone camera records movement on the MRI screen and movement of a paper tag (gray) attached to the string. A single frame from the resulting video is shown on the top right.

Part **B** illustrates how the resulting video is processed: The video is segmented, and the obtained object velocity curves are cross-correlated to obtain the delay between both movements.

S3 Real-Time MRI Reconstruction Videos

Corresponding video for Figure 5, covering three heartbeats, starting at the same time as the timeseries shown in Figure 5. The ordering matches the original figure, that is, images were reconstructed using (from left to right) the fast, good, and high-quality settings of the `rtreco.sh` reconstruction script.